Thin Solid Films 517 (2009) 1515–1521

Contents lists available at ScienceDirect

Thin Solid Films

journal homepage: www.elsevier.com/locate/tsf

The Leidenfrost effect during spray pyrolysis of nickel oxide-gadolinia doped ceria composite thin films

Ulrich P. Muecke [a,*], Gary L. Messing [b,1], Ludwig J. Gauckler [a,2]

[a] ETH Zurich, Department of Materials, Nonmetallic Inorganic Materials, Wolfgang-Pauli-Str. 10, CH-8093 Zurich, Switzerland
[b] Pennsylvania State University, Materials Science and Engineering, 121 Steidle Bldg., University Park, PA 16802, USA

ARTICLE INFO

Article history:
Received 13 October 2006
Received in revised form 22 June 2008
Accepted 12 August 2008
Available online 27 August 2008

Keywords:
Ceramics
Deposition process
Evaporation
Organic substances
Nickel oxide
Cerium gadolinium oxide
Yttria stabilized zirconia
Boiling point

ABSTRACT

$NiO–Ce_{0.8}Gd_{0.2}O_{1.9-x}$ (CGO) thin films were prepared by air blast spray pyrolysis with precursors containing nickel nitrate, cerium nitrate and gadolinium chloride in ethanol and a high boiling point organic solvent. Precursors containing solvents with boiling points between 120 and 314 °C were sprayed on sapphire, silicon, Foturan®, yttria stabilized zirconia and CGO at different substrate surface temperatures.
A maximum deposition temperature, above which film deposition ceased completely, was observed. The limiting temperature for film formation was correlated with the Leidenfrost phenomenon. At temperatures above the Leidenfrost point of the precursor, the sprayed droplets do not impact and spread on the substrate surface but levitate on a vapour cushion above the substrate and are swept away by the air stream. The Leidenfrost point of a precursor was found to depend on the solvent boiling point, the metal salt concentration and the thermal properties of the substrate expressed as the product of density, thermal conductivity and heat capacity. The maximum deposition temperature increased with increasing solvent boiling point or metal salt concentration and with decreasing product of density, thermal conductivity and heat capacity of the substrate.

1. Introduction

Spray pyrolysis of ceramic thin films involves the atomization of a liquid precursor, droplet transport towards a heated substrate, droplet impact, spreading of the liquid droplets on the substrate, evaporation of the solvent and decomposition of the deposited material [1]. Crack-free films can be obtained when the deposition temperature is above the precursor boiling point [1]. Beckel et al. [2] reported a limiting substrate surface temperature above which no continuous films can be obtained. The phenomenon was explained by an increasing number of solidified droplets due to solvent evaporation that are blown away by the air stream.

However, experimental observations of this work suggest that additional mechanisms like the Leidenfrost phenomenon [3–5] might also influence the limiting substrate temperature. When a droplet of a pure substance is deposited on a hot substrate at a temperature below the boiling point of the liquid, the droplet wets the substrate, spreads and slowly evaporates. At temperatures above the boiling point, the droplet wets the surface, spreads, vapour bubble nucleation occurs within the liquid, the droplet boils and vanishes after a short period of time. Eventually the substrate temperature becomes sufficiently high that a thin vapour layer is formed at the interface and the droplet levitates above its own vapour. This point is called the Leidenfrost point (LFP). The droplet lifetime increases by orders of magnitude at this point because of the insulating properties of the vapour layer. When the droplet is not deposited slowly but arrives with a certain initial velocity the impact dynamics also have to be taken into consideration [3]. Metal salts, salt decomposition intermediates or oxidic solids can precipitate in the droplet during evaporation for precursors containing metal salts [2].

The aim of this paper is to correlate film formation parameters and the observation of a maximum deposition temperature on sapphire with the Leidenfrost phenomenon and to extend this correlation to various substrate materials. The spray process was studied for the production of nickel oxide–cerium gadolinium oxide (NiO–CGO) thin films which can be used as anodes for miniaturized solid oxide fuel cells [6].

2. Experimental details

2.1. Spray pyrolysis setup

A schematic of the spray pyrolysis setup is given elsewhere [2]. In this study, the liquid precursor solution was fed with a glass/teflon® syringe (model 1050, Hamilton, Reno, NV, USA) and a syringe pump (model A-99, Razel, St. Albans, VT, USA) through a viton hose (Masterflex/Cole-

* Corresponding author. Tel.: +41 44 633 6841; fax: +41 44 632 1132.
E-mail addresses: ulrich.muecke@mat.ethz.ch (U.P. Muecke), messing@ems.psu.edu (G.L. Messing), ludwig.gauckler@mat.ethz.ch (L.J. Gauckler).
[1] Tel.: +1 814 865 2262; fax: +1 814 865 8262.
[2] Tel.: +41 44 632 5646; fax: +41 44 632 1132.

0040-6090/$ – see front matter © 2008 Published by Elsevier B.V.
doi:10.1016/j.tsf.2008.08.158

Table 1
Solvents used for the preparation of the precursors

Solvent	Abbreviation	Boiling point [°C]	Purity
Ethanol[1]	E	78	99.8%
1-Methoxy-2-propanol[2]	MP	119–121	99%
n-Butyl acetate[2]	BA	124–126	98.5%
Diethylene glycol[3]	DEG	245	99%
Diethylene glycol dimethyl ether[2]	DEG DME	162	99%
Diethylene glycol monoethyl ether[2]	DEG MEE	195	98%
Diethylene glycol mono *n*-butyl ester acetate[2]	BCA	245	98%
Triethylene glycol[3]	TEG	285	99%
Adipic acid di *n*-butyl ester[4]	ASDBE	305	96%
Tetraethylene glycol[4]	4EG	314	99%

Suppliers: [1]Merck, Darmstadt, DE and Scharlau, Barcelona, ES; [2]Fluka, Buchs, CH; [3]Acros, Geel, BE; [4]Aldrich, Steinheim, DE; all boiling point data from suppliers.

Parmer, Vernon Hills, IL, USA) to a spray gun (model Binks 460 with a J92P air nozzle and a J920 fluid nozzle, Binks/ITW, Glendale Heights, IL, USA). The fluid needle of the spray gun was in the fully open position and the fan spray width adjustment in the fully closed position for all experiments, resulting in a circular spot deposition of approximately 5 cm diameter at 39 cm working distance and 0.1 MPa air pressure. The air pressure was adjusted with a pressure regulator (EAR 2000, SMC, JP and Norgren/IMI, Birmingham, UK) to a precision of ±5 kPa.

A glass ceramic hot plate (model CT10 with 1.8 kW, Harry Gestigkeit GmbH, Düsseldorf, DE) was used for heating the substrates. A circular aluminium plate of 150 mm diameter and 6 mm thickness was placed on the hot plate to ensure temperature homogeneity of better than 1 °C over the sprayed area. The plate was polished before each experiment with silicon carbide abrasive paper grade 1200 to eliminate strong radiative heat transfer from black residues to the sprayed droplets and to ensure temperature homogeneity by good thermal contact with the substrate. The temperature of the aluminium plate was adjusted with a 1 mm diameter type K thermocouple (MTS Messtechnik, Schaffhausen, CH) and a temperature controller (model 3216, Eurotherm, West Sussex, UK) to limit temperature fluctuations over time to less than ±0.5 °C. The thermocouple was situated in a hole parallel to the plate surface with the tip in the centre underneath the substrate. All substrate surface temperature measurements were carried out with a calibrated handheld surface probe of type K (Model 88108, Omega, Stamford, CT, USA). The error for substrate temperature measurements under flowing air was estimated to be ±5 °C with a reproducibility better than ±2 °C, and without air flow ±2 °C with a reproducibility better than ±1 °C. The greatest care has to be exerted in substrate placement and temperature measurement as temperature changes of 10 to 20 °C can result in a doubled film growth rate under certain conditions.

2.2. Characterization

The morphologies of the deposited films were analyzed with a light microscope equipped with a digital camera (Polyvar MET and Leica DC300, Reichert-Jung/Leica Microsystems, Wetzlar, DE). Film thicknesses were measured by scratching off a small portion of the film with a scalpel and measuring the step height between the substrate and an averaged height within about 1 mm scan length of the film with a surface profiler (Alpha Step 500, KLA Tencor, San Jose, CA, USA). Surface tensions were measured at 25 °C in a saturated environment with a profile analysis tensiometer (PAT-1, SInterface, Berlin, DE). Droplet volume distributions of the spray were measured with a laser diffraction droplet size analyzer (Helos, Sympatec, Clausthal-Zellerfeld, DE). Viscosities were measured at 20 °C in the shear rate range from 5 to 200 s^{-1} with a rheometer (Gemini with DG 24/27 Ti double gap measurement system, Bohlin/Malvern, Worcestershire, UK).

Temperatures of the air stream between the heating plate and the spray gun were measured with a 1 mm diameter type K thermocouple placed horizontally with the tip in the centreline of the air stream.

2.3. Precursor composition and properties

The liquid precursors consisted of a mixture of ethanol and one or more higher boiling point solvents as well as metal salts in the desired stoichiometry. The metal salts were dissolved in ethanol under stirring and after complete dissolution the higher boiling point solvents were added. The total concentration of all metal salts was 0.1 mol/l with an intended composition of the final layer of 60 vol.% metallic nickel and 40 vol.% $Ce_{0.8}Gd_{0.2}O_{1.9-x}$. The ceramic film itself was deposited in the oxidic state as a mixture of NiO and CGO. Nickel-II-nitrate hexahydrate (98% purity, Fluka, Buchs, CH), cerium-III-nitrate hexahydrate (99.5%, Alfa Aesar, Karlsruhe, DE) and gadolinium-III-chloride hexahydrate (99.9%, Alfa Aesar) were used for all spray solutions with 2.46 g, 0.54 g and 0.115 g respectively dissolved per 100 ml of total solvent volume. The crystal water content and resulting molar mass of the salts were verified by thermogravimetry before the solution preparation. Table 1 gives an overview of all solvents used throughout this work with the respective boiling points, purities, suppliers and abbreviations. All solvents were completely miscible with ethanol in a volume ratio of 1:9.

The liquid properties of primary importance for spray generation are density, viscosity and surface tension [7]. Measured values for viscosities and surface tensions of the pure solvents, the solvent mixtures and two precursors are given in Table 2. All liquids exhibited Newtonian behaviour in the investigated range. The viscosity of the 1:9 E:4EG precursor with metal salts was stable to ±5% of the initial value over a period of 4 weeks. Adding metal salts to the solvent had almost no influence on surface tension and only a slight influence on viscosity. Consequently, a measured droplet distributions of solvent mixtures without salts should reflect the distribution during spraying of precursors with salts.

2.4. Substrate materials

Sapphire single crystals (Stettler, Lyss, CH) with a $(11\bar{2}0)$ orientation parallel to the surface, a diameter of 10 mm and a thickness of 1 mm were used as substrates. Small pieces with a size of approximately 10×10 mm^2 of tape-cast polycrystalline 8-YSZ $(Y_2O_3)_{0.08}(ZrO_2)_{0.92}$ with a thickness of 500 μm (Kerafol, Stegenthumbach, DE), Foturan® in the

Table 2
Surface tensions and viscosities of solvents, solvent mixtures and precursors

Solvent or solvent mixture [volume ratios]	Surface tension at 25 °C [$\times10^{-3}$ N/m]	Viscosity at 20 °C [$\times10^{-3}$ Pas]
Ethanol	21.8 [22]	1.2
Water	72.0	1.0
1:1:1 E:MP:BCA	25.9	2.1
1:1:1 E:MP:BCA with salts 0.1 mol/l	25.7	–
BA	25.1[a]	0.74 at 25 °C[a]
1:9 E:BA	26.5	1.3
DEG	48.2	38.5
1:9 E:DEG	39.1	21.2
DEG DME	29.5[a]	0.99 at 25 °C[a]
1:9 E:DEG DME	30.5	1.7
DEG MEE	29.5[a]	3.9 at 25 °C[a]
1:9 DEG MEE	–	3.9
BCA	30[a]	3.02 at 25 °C[a]
1:9 E:BCA	29.1	2.5
TEG	45.2[a]	49[a]
1:9 E:TEG	39.6	25.9
4EG	44.1[a]	44.6 at 25 °C[a]
1:9 E:4EG	40.2	35.5
1:9 E:4EG with salts 0.1 mol/l	40.6	38.0

[a] Data of pure substances taken from [27].

Table 3
Properties of the substrate materials

Substrate material	Surface roughness r_A [Å]	Density ρ [g/cm^3]	Heat capacity c_p [J/kg K]	Thermal conductivity λ [W/m K]	$\lambda\rho c_p$ [×10^6 W^2 s/m^4 K^2]
Sapphire	8.1	3.99[a]	750 at 25 °C[a]	~40 at 25 °C [8]	120
YSZ	546	5.85[a]	465 at 25 °C [26]	2.2 at 25 °C [9] ~6.5 at 25 °C for pure monoclinic ZrO_2 [10]	6
CGO	20.1	>6.93	n. a.	~12 for pure CeO_2 at 400 °C [11]	n. a.
Foturan® (glass)	32.1	2.37[a]	878 at 25 °C[a]	1.35 at 20 °C[a]	2.8
silicon wafer	0.0	2.33[a]	710[a]	160[a]	265

[a] Data from supplier.

glassy state (Mikroglas, Mainz, DE) with a thickness of 300 μm and polished $Ce_{0.8}Gd_{0.2}O_{1.9-x}$ (CGO) pellets with a thickness of 2 mm and exceeding 95% of the theoretical density (ρ_{th} = 7.29 g/cm^3) were also used. The surface roughnesses of all materials are given in Table 3. The r_A values were measured along a scan length of 50 μm. All substrates were cleaned with ethanol prior to deposition.

3. Results and discussion

3.1. Droplet size distribution and flow field

The effect of air pressure and type of fluid on the droplet volume distribution was measured for the Binks 460 spray gun. Ethanol, water and a mixture of 1:1:1 E:MP:BCA without metal salts were used as model precursors with different surface tensions and viscosities. The air pressure was kept at 0.1 MPa except for ethanol where it was varied between 0.04 and 0.14 MPa in steps of 0.04 MPa. The liquids were fed through the nozzle at ambient pressure and a flow rate of 30 ml/h.

Fig. 1 shows the droplet volume distributions recorded at a distance of 3 mm from the tip of the spray nozzle. In accordance to earlier findings [12], the majority of the sprayed precursor volume was transported by droplets with diameters between 5 and 50 μm with the maximum of the volume distribution being at droplet diameters between 10 and 20 μm. The volume fraction of larger droplets increased with decreasing air pressure for pure ethanol. The droplet volume distributions shifted towards larger droplets with increasing viscosity or surface tension of the liquid. A variation of the flow rate between 5 and 120 ml/h had no influence on the volume distribution. The atomization process was, therefore, only dependent on the air pressure and type of liquid in the flow rate range investigated.

3.2. Maximum deposition temperature

The substrate surface temperature is one of the most important parameters in spray pyrolysis. Continuous films can be prepared in a temperature interval between a lower deposition temperature and a maximum deposition temperature. Discontinuous films are formed at surface temperature below the lower deposition limit [13] and the deposition ceases completely above the maximum deposition temperature. Precursor solutions with different high boiling point solvents were sprayed on sapphire at different temperatures to obtain a quantitative correlation between the boiling point of the high boiling point solvent, substrate surface temperature and the maximum deposition temperature.

In this study, the maximum deposition temperature was defined to be the temperature at which the coverage was incomplete and only single separated residues were deposited on the substrate surface after 60 min of deposition at 30 ml/h. The solvent volume ratios were chosen to be 1:9 ethanol:high boiling point solvent so that the physical properties of the precursors where mainly defined by the properties of the high boiling point solvent. The flow rate was 30 ml/h, the spray time between 1 and 60 min, the working distance 39 cm and the air pressure 0.1 MPa.

A linear relation between the boiling point of the high boiling point solvent and the maximum deposition temperature was observed for all solvent boiling points above approximately 200 °C (Fig. 2). The maximum deposition temperature was approximately 95–115 °C higher than the boiling point for every solvent in this range and became independent of the solvent for boiling points below 200 °C. The visual appearance of the films changed from brownish-black to light green at 200 °C, indicating a change in the type of residue formed on the substrate surface. Nickel nitrate decomposes over a number of

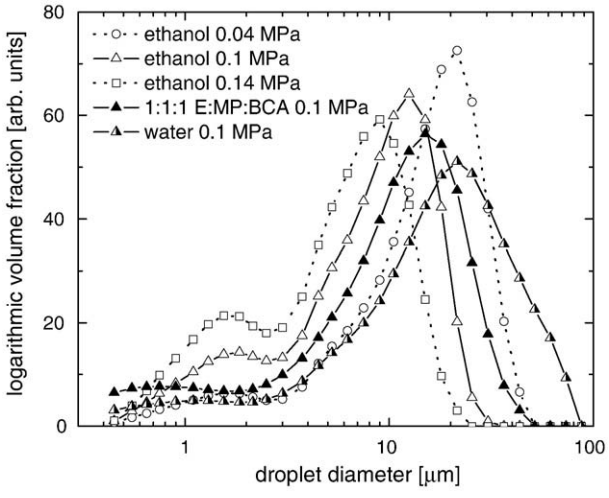

Fig. 1. Logarithmic droplet volume distribution of the Binks 460 spray gun for different solvents as a function of atomization pressure.

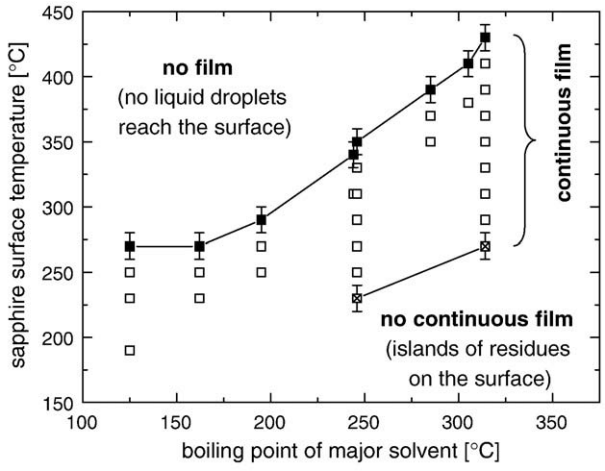

Fig. 2. Film formation behavior on sapphire as a function of substrate temperature and solvent boiling points for 0.1 M precursors with 1:9 ethanol:high boiling point solvent (lines are guidance for the eyes only; the boiling point of BCA and DEG is 245 °C, values are plotted with an offset for improved clarity).

nickel nitrate hydrate intermediates to a relatively stable green-coloured compound at around 250–300 °C. The green colour of the film stems most probably from the presence of such an intermediate. The decomposition then proceeds to black nickel oxide at higher temperatures [14].

The maximum deposition temperature decreased by 10 to 20 °C when the salt concentration was lowered from 0.1 mol/l to 0.01 mol/l. Increasing the ethanol to DEG ratio from 1:9 to 1:2 and 2:1 decreased the maximum deposition temperature from 350 °C to 340 °C and 330 °C, respectively.

The optimum spray temperature interval for the preparation of crack-free films with maximum thickness was about 20–40 °C below the maximum deposition temperature for all precursors [13]. Decreasing the substrate temperature from 40 °C below the maximum deposition temperature towards the lower deposition limit resulted in a gradual reduction of the maximum possible crack-free film thickness of ~800 nm to 200–300 nm. The maximum crack-free film thickness of the DEG DME-based precursor was 200–300 nm at 270 °C, 300–400 nm at 330 °C for the DEG-based precursor and 800 nm at 390 °C for the 4EG-based precursor. It was not possible to produce crack-free films thicker than 200–300 nm with solvents of boiling points lower than 200 °C. Therefore, the discussion will focus on films produced at substrate temperatures above 300 °C and with precursors with solvents of boiling point higher than 200 °C.

The lower deposition limit was characterized by large disconnected islands of residues on the surface with no continuous film in between. The lower deposition temperature was 230 °C for the DEG-based precursor and 270 °C for the 4EG-based precursor.

3.3. Substrate material

The maximum deposition temperature was not only a function of the boiling point of the majority solvent but also strongly depended on the substrate material. Sapphire was exchanged with YSZ, CGO, silicon and Foturan® and a precursor with 1:9 E:4EG was sprayed at a flow rate of 5 ml/h, a working distance of 39 cm and an air pressure of 0.1 MPa. The maximum deposition temperature was found to be 430±10 °C on sapphire, 500±10 °C on YSZ, 490±10 °C on CGO, 390±10 °C for silicon and >470 °C on Foturan®. At higher temperatures, Foturan® started to soften and warp, resulting in non-homogenous surface temperatures and deposition conditions.

The film thickness on all substrate materials and for all temperatures increased linearly with the spray time (Fig. 3). The deposition rates increased with decreasing substrate surface temperature for all substrates (Fig. 4) and increased linearly with the flow rate within the range of 5 to 30 ml/h (not shown). The deposition rates at the same surface temperature differed by ~500 nm/h between sapphire and CGO, YSZ or Foturan®. Films with thicknesses above ~800 nm were cracked after deposition on all substrate materials with the 1:9 E:4EG based precursor [13].

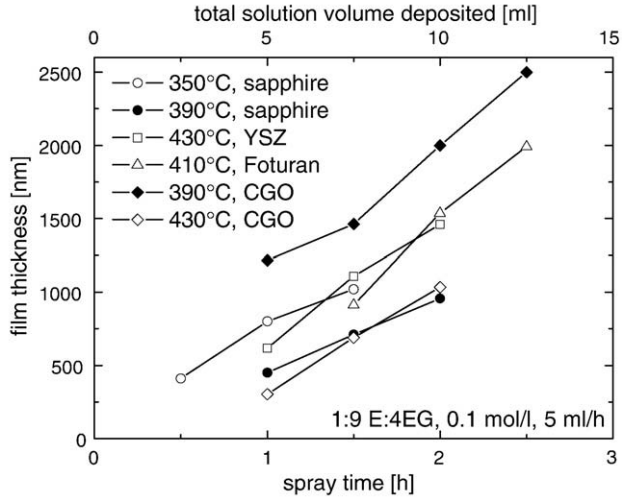

Fig. 3. Film thickness as a function of spray time on different substrate materials.

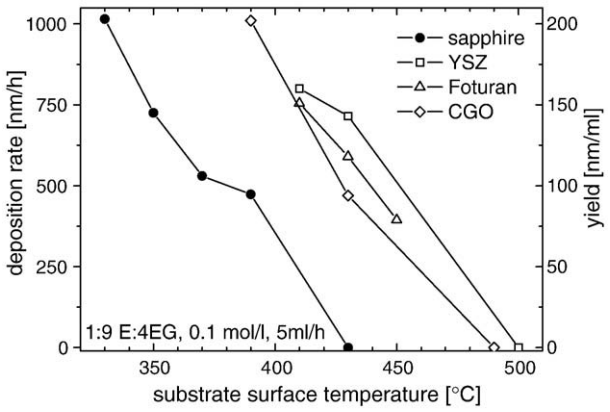

Fig. 4. Deposition rates as a function of substrate temperature on different substrate materials.

To explain the varying deposition rates on different substrates and the observation of a substrate and solvent boiling point dependent maximum deposition temperature, the droplet movement, impact and evaporation behavior have to be taken into consideration.

3.4. Droplet dynamics, impact and evaporation

3.4.1. Working distance

Fig. 5 shows images of the initial stages of deposition for a precursor of 1:1:1 E:MP:BCA at working distances of 20, 30 and 39 cm. The substrate was sapphire, the temperature 330 °C, the flow rate 30 ml/h and the deposition time 5 min. The deposition rates increased with decreasing working distance and a large number of small splats (encircled in Fig. 5a) with diameters of 0.5–2 μm and large splats with diameters around 5–10 μm (arrowed in Fig. 5b) can be distinguished on the substrate and within the film. Splats are porous, half-dome shaped deposits from droplets that did not spread completely after impact [13]. At 39 cm working distance, only large residues with diameters >10 μm were found and splats were rarely observed. Repetitive deposition of residues leads to the formation of a continuous and homogenous film. The presence of splats deteriorates the film quality because additional porosity is introduced in the film. The diameter of the residues increased for precursors with increasing viscosities and surface tensions as a result of an increased number of larger droplets in the spray (Fig. 1).

The trajectory of two droplets with different sizes moving in an air stream impinging on a heated plate is sketched in Fig. 6. After leaving the spray nozzle all droplets are transported under the influence of gravitational and drag forces and follow the flow paths of the air stream. Thermophoresis is negligible at that distance because the temperature gradient of the air stream is insignificant (Fig. 7). The impinging gas stream is redirected sideways while approaching the heating plate, creating a flow parallel to the substrate and directed outwards. Assuming the same initial velocity for the small and the large droplets, sufficiently small droplets will be entrained by the flow whereas the large droplets have sufficient inertia to be deposited. Increasing the droplet velocity by decreasing the working distance therefore results in the impingement of a larger number of small droplets on the substrate. Solvent evaporation is faster from smaller precursor droplets, resulting in a large number of small splats at a working distance of 20 cm and a decreasing number of splats with increasing working distance.

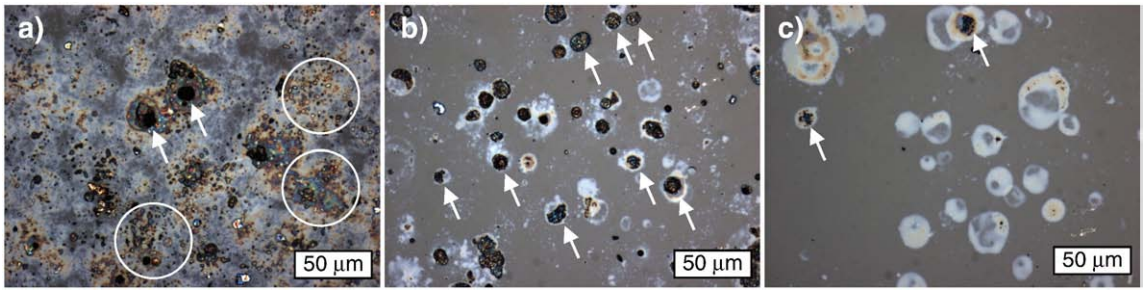

Fig. 5. Light microscope images of the initial stages of deposition at (a) 20 cm, (b) 30 cm and (c) 39 cm working distance. Examples of small splats with diameters around 1 µm are encircled and of large splats with diameters around 10 µm are arrowed.

Changing the working distance therefore provides a means of reducing the number of small droplets and splats or by selectively removing the lower fraction of the droplet volume distribution. Splat formation can also be suppressed in the idealized case of a spray gun with a monodispersed droplet size distribution.

3.4.2. Thermophoresis

The temperature gradient along the flight path of the droplets also influences the deposition properties. Fig. 7 shows the air temperature as a function of distance from the heating plate surface above a 1 mm thick circular sapphire substrate with a diameter of 35 mm and a 300 µm thick square 25×25 mm^2 YSZ substrate. The substrate surface temperature was 390 °C, the precursor flow rate 0 ml/h and the air pressure 0.1 MPa for both materials. The convective heat transfer by the gas stream leads to a steep temperature profile with a sharp increase of air temperature within the last 3 mm above the substrate surface. The temperature gradients above YSZ and sapphire were similar.

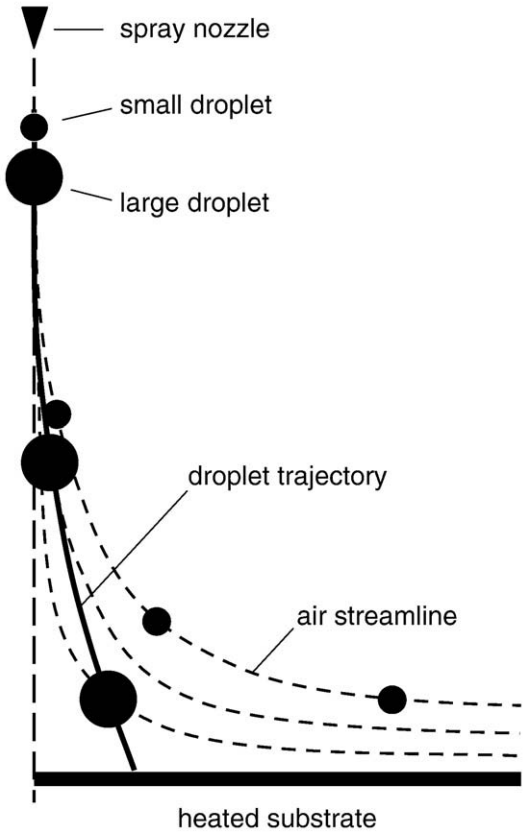

Fig. 6. Schematic of two droplets with different sizes moving in an air stream towards a heated substrate.

A thermophoretic force is imposed on droplets close to the substrate by the temperature gradient. The force is directed vertically upwards, is proportional to the temperature gradient along the flight path and acts strongest on droplets with a large cross-sectional area to volume ratio, i. e. small droplets. As a consequence, droplets slowed down within the last millimetres above the surface because of the redirection of the air stream (Fig. 6) and with just enough inertia to be deposited on a cold substrate would then not be deposited due to the thermophoretic forces and the deposition rate would decrease with increasing temperature.

To compare the magnitude of the thermophoretic force with the gravitational and the drag force, the drag force on a single droplet in the impinging air stream was assumed to be equal to the drag force on a droplet moving in an undisturbed air stream with the same gas velocity as the impinging stream [15].

The magnitudes of the thermophoretic force F_T [16]

$$F_T = 9 \cdot \pi \cdot \frac{d_d}{2} \cdot \frac{\eta_a^2}{\rho_a \cdot T_a} \cdot \left(\frac{\lambda_a}{2\lambda_a \cdot \lambda_d} \right) \cdot \mathrm{grad}(T)$$

the drag force F_D [17]

$$F_D = \frac{1}{6} \cdot \pi \cdot \rho_d \cdot d_d^3 \cdot g$$

and the gravitational force F_G

$$F_G = 6 \cdot \pi \cdot \eta_a \cdot v_d \cdot \frac{d_d}{2}$$

are compared in Table 4 as a function of the droplet diameter d_d. The viscosity of air η_a, density of the air ρ_a, the thermal conductivities of

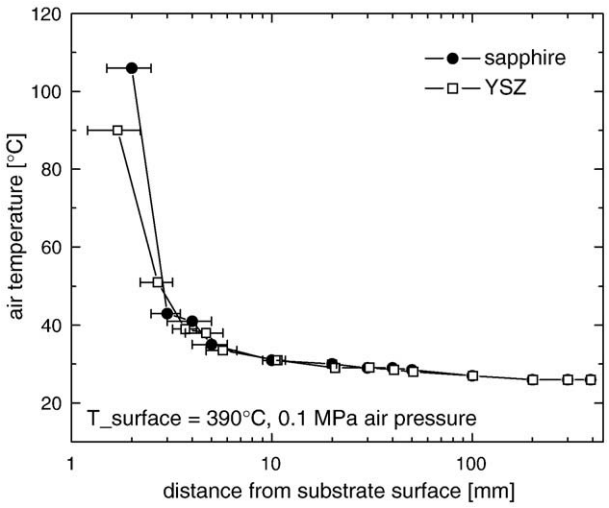

Fig. 7. Temperature profile between the spray nozzle and the heating plate for a sapphire and a YSZ substrate.

Table 4
Comparison of the thermophoretic force, drag force and gravitational force as a function of droplet diameter

Droplet diameter [μm]	Thermophoretic force [N]	Drag force [N]	Gravitational force [N]
1	$1.1 \cdot 10^{-13}$	$1.7 \cdot 10^{-10}$	$4.1 \cdot 10^{-15}$
10	$1.1 \cdot 10^{-12}$	$1.7 \cdot 10^{-9}$	$4.1 \cdot 10^{-12}$
100	$1.1 \cdot 10^{-11}$	$1.7 \cdot 10^{-8}$	$4.1 \cdot 10^{-9}$

the air λ_a and the droplet λ_d, the air temperature T_a, the air temperature gradient grad(T), the density of the droplet ρ_d and the acceleration of gravity g were estimated to be $18 \cdot 10^{-6}$ kg/m s, 1.2 kg/m^3, 0.025 W/m K, 0.18 W/m K, 663 K, 350 K/$2 \cdot 10^{-3}$ m (Fig. 7), 800 kg/m^3 and 9.81 m/s^2, respectively. The velocity of the droplet v_d before impact was assumed to be the same as that measured by Wilhelm et al. [12] in a similar spray setup and equal to 1 m/s.

Thermophoretic forces of droplets with diameters of <10 μm are 2 to 3 orders of magnitude smaller than drag forces. The effect of thermophoretic forces on the droplet flight path compared to drag and inertia forces is therefore hard to estimate and the relative contribution of thermophoresis remains unclear. Additionally, thermophoresis cannot explain the different maximum deposition temperatures on the various substrate materials under the assumption of similar emissivities of the different substrate materials.

3.5. Leidenfrost phenomenon

The behaviour of a liquid droplet impacting on a hot surface is also strongly influenced by the Leidenfrost phenomenon. The parameters influencing the Leidenfrost point (LFP) for droplets are initial volume, impact velocity, surface tension of the liquid, liquid boiling point and the presence and concentration of salts in the liquid. Those related to the substrate surface are surface roughness and thermal diffusivity, and for the interaction of the liquid with the solid, the influencing parameter is the wetting angle of the fluid on the substrate [18]. The spreading behaviour and the droplet shape after impact are also related to these variables [19].

According to Bernardin et al. [19,20] the LFP of a pure liquid is independent of the initial volume, surface roughness and impact velocity. The LFP of heptane and water droplets is insensitive to the droplet size within the range of 68 μm to 314 μm and 0.4 to 1.8 mm respectively [21]. Therefore, the LFP of droplets in the spray should be comparable to that of millimetre-sized droplets and experiments with macroscopic droplets were used to investigate the influence of the Leidenfrost phenomenon on the deposition process.

3.5.1. Influence of wetting angle

Nagai et al. [22] reported that differences in wettability of a fluid on a substrate results in differences in the LFP. The results of Bernardin et al. [5] contradict these findings and the authors state that the LFP is fairly insensitive to wetting characteristics. The wetting angle of a liquid on a solid material is a function of temperature and of the presence of surface impurities [23]. A qualitative experiment was performed to assess the wetting behaviour of the spray solutions on different substrate materials. Sapphire, CGO and YSZ samples were placed on the heating plate at 390 °C for 5 min, cooled rapidly to room temperature and either a drop of 1:9 E:4EG or 1:9 E:BCA without salts were deposited by means of a pipette on each of the surfaces. Complete spreading of the millimetre-sized droplets to a diameter of 30 mm up to the edges of the substrates was observed, indicating a similar wetting angle for the solvent mixtures. The influence of the wetting angle on the LFP will therefore be neglected in the following, although an effect cannot be excluded completely because of the temperature dependency of the wetting angle.

3.5.2. Influence of solvent and metal salts

The LFPs on sapphire and on YSZ of the pure solvents 4EG, DEG, BCA and DEGMEE, the mixtures with ethanol in a 1:9 ratio without salts and the respective precursors with a 0.1 M and 0.01 M concentration were measured by manually depositing a droplet from a distance of 20 mm on the substrate with a pipette in still air (see Table 5).

At temperatures much below the Leidenfrost point, where the droplet lifetime reached several seconds, all pure solvents evaporated calmly without boiling. Two distinct boiling regimes were distinguishable when 10 vol.% ethanol were added to the pure solvent. Vigorous boiling was observed in the first second, followed by a period of calm evaporation. When approaching the Leidenfrost point, the two regimes were not distinguishable any more and all tested liquids evaporated under heavy bubbling.

The measured LFPs of all precursors except for DEG MEE are in excellent agreement with the maximum deposition temperatures found on sapphire (Fig. 2) and it can be concluded that the Leidenfrost phenomenon limits the range of possible deposition temperatures during spray pyrolysis for precursors with solvent boiling points between 195 and 314 °C.

The small differences of the LFPs between DEG and BCA, which have the same boiling point, is most likely due to the differences in liquid surface tension [24].

The LFP of all 0.1 M precursors was 20–30 °C higher than for the pure solvent mixture. Decreasing the salt concentration from 0.1 M to 0.01 M decreased the LFP by 5–20 °C to a level between that of the pure solvent mixture and the 0.1 M precursors, explaining the difference of 10–20 °C in maximum deposition temperature between a 0.1 and a 0.01 M precursor. The Leidenfrost point did not change when ethanol was replaced by water in a 0.1 M precursor with 1:9 E/W:4EG.

It is important to note that the LFP does not only depend on the solvent boiling point and salt concentration but also on the type of salt. The LFP of a 0.1 M precursor of zirconium oxynitrate hexahydrate and yttrium nitrate hexahydrate in 1:9 W:4EG for the preparation of a 8 mol% yttria doped zirconia thin film was 350–370 °C compared to 430 °C for NiO–CGO.

3.5.3. Influence of substrate material

Baumeister et al. [24] pointed out that the parameter $\lambda \cdot \rho \cdot c_p$ of the substrate material (see Table 3) is important in the determination and prediction of the Leidenfrost point. The area under an impacting droplet cools much more for a material with low values of heat capacity, density and heat conductivity than for a material with high

Table 5
Measured Leidenfrost points of solvents, solvent mixtures and precursors on sapphire and YSZ

Solvent, solvent mixture or precursor	Max. dep. temp. on sapphire [°C]	LFP on sapphire [°C]	LFP on YSZ [°C]
4EG pure (b. p. 314 °C)		500±10	
1:9 E:4EG		405±5	
1:9 E:4EG with salts 0.1 mol/l	430±10	435±5	
1:9 E:4EG with salts 0.01 mol/l		420±5	
DEG pure (b. p. 245 °C)		455±10	
1:9 E:DEG		350±10	>390 °C
1:9 E:DEG with salts 0.1 mol/l	350±10	370±10	
1:9 E:DEG with salts 0.01 mol/l	340±10	365±5	
BCA pure (b. p. 245 °C)		375±10	
1:9 E:BCA		310±5	>390 °C
1:9 E:BCA with salts 0.1 mol/l	340±10	330±5	
1:9 E:BCA with salts 0.01 mol/l		325±5	
DEG MEE pure (b. p. 195 °C)		310±10	
1:9 E:DEG MEE		300±5	
1:9 E:DEG MEE with salts 0.1 mol/l	290±10	330±5	
1:9 E:DEG MEE with salts 0.01 mol/l		310±5	

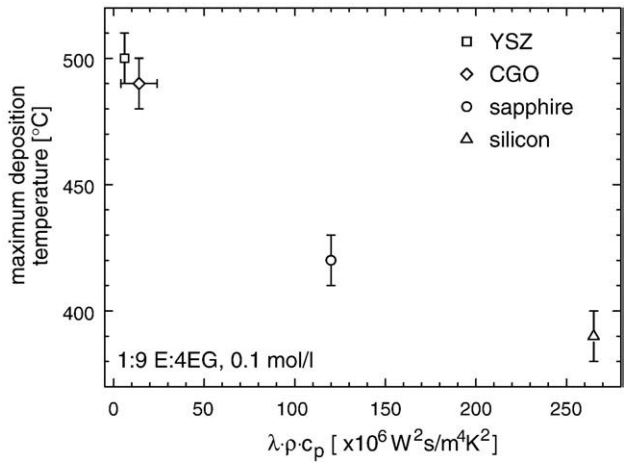

Fig. 8. Correlation of the maximum deposition temperature on various substrate materials with the products of the thermal conductivity λ×the density ρ×the heat capacity c_p of the substrate.

thermal conductivity and large heat capacity because of the different heat fluxes through the solid towards the impact zone. The formation of a vapour cushion and onset of levitation is shifted towards higher temperatures for materials with low density, thermal conductivity and heat capacity [25].

The Leidenfrost points on a YSZ substrate were determined for two solvent mixtures of 1:9 E:DEG and 1:9 E:BCA without metal salts and were found to be higher than 390 °C for both mixtures, compared to 350 and 310 °C respectively on sapphire.

Fig. 8 shows the maximum deposition temperature as a function of $\lambda \cdot \rho \cdot c_p$ for YSZ, CGO, sapphire and silicon. The coefficient of heat capacity of CGO was approximated to be same as that of YSZ and the heat conductivity to be twice that of YSZ (see Table 3) and a value of $\lambda \cdot \rho \cdot c_p$ of $14 \pm 10 \times 10^6$ W^2 s/m^4 K^2 was assumed. Futuran® was not included because of the uncertainty of maximum deposition temperature due to softening at temperatures >470 °C.

The maximum deposition temperatures clearly depend on $\lambda \cdot \rho \cdot c_p$. This correlation is expected to hold not only for the investigated substrates but for any substrate material under similar experimental conditions.

3.5.4. Consequences for film formation

The maximum deposition temperature for a new precursor on any substrate can be determined by measuring the LFP of a macroscopic droplet of the precursor on the desired substrate material. If a precursor containing nickel, cerium or gadolinium salts or a combination thereof is used, the maximum deposition temperature can be extrapolated from the data given in Figs. 2 and 8.

The deposition temperature of a given precursor with known deposition parameters on a specific substrate material can be approximated to new substrate materials by extrapolating the difference in maximum deposition temperature between the substrates from Fig. 8.

Spraying a metal oxide thin film with a $\lambda \cdot \rho \cdot c_p$ different than the substrate material will also result in a changing deposition rate with time because the deposited film forms a thermally more conductive or more insulating layer between the droplet and the substrate.

4. Summary and conclusion

Precursor solutions with different high boiling point solvents were sprayed on different substrates at varying surface temperatures. The deposition rates changed with substrate surface temperature, high boiling point solvent and substrate material. A maximum deposition temperature above which deposition ceases completely was found for each precursor. This temperature was a function of solvent boiling point and substrate material.

The dependence of the maximum deposition temperature on solvent boiling point was ascribed to the Leidenfrost phenomenon. Droplets deposited above the Leidenfrost point levitate on a vapour cushion and are swept away by the air stream during deposition. The Leidenfrost temperature of the investigated precursors was in good agreement with the maximum deposition temperatures.

The differences in maximum deposition temperature between substrate materials are also a consequence of the Leidenfrost phenomenon and were correlated to the thermal properties of the substrates, expressed as the product of density, thermal conductivity and heat capacity. For materials with good thermal conductivity, large heat capacity or high density, like metals and semiconductors the maximum deposition temperature is lower compared to materials with low values of thermal conductivity, heat capacity and density, e.g. for ceramics.

Acknowledgment

Financial support from BFE under project number 100430, from KTI under project number 7085.2 DCPP-NW, from the European Union within the REAL-SOFC project and from ETH Zurich is gratefully acknowledged. The authors would like to thank Kerafol (Stegenthumbach, DE) for the generous supply with tape-cast YSZ substrates.

References

[1] D. Perednis, L.J. Gauckler, J. Electroceramics 14 (2005) 103.
[2] D. Beckel, A. Dubach, A.R. Studart, L.J. Gauckler, J. Electroceramics 16 (2006) 221.
[3] B.S. Gottfried, C.J. Lee, K.J. Bell, Int. J. Heat Mass Transfer 9 (1966) 1167.
[4] J.D. Bernardin, I. Mudawar, J. Heat Transfer 126 (2004) 272.
[5] J.D. Bernardin, I. Mudawar, J. Heat Transf.-Trans. ASME 121 (1999) 894.
[6] A. Bieberle-Hütter, D. Beckel, U.P. Muecke, J.L.M. Rupp, A. Infortuna, L.J. Gauckler, Mst news 4-05 (2005) 12.
[7] P.H. Marmottant, E. Villermaux, J. Fluid Mech. 498 (2004) 73.
[8] S. Burghartz, B. Schulz, J. Nucl. Mater. 215 (1994) 1065.
[9] D.P.H. Hasselman, L.F. Johnson, L.D. Bentsen, R. Syed, H.L. Lee, M.V. Swain, Am. Ceram. Soc. Bull. 66 (1987) 799.
[10] S. Raghavan, H. Wang, R.B. Dinwiddie, W.D. Porter, M.J. Mayo, Scr. Mater. 39 (1998) 1119.
[11] V.Y. Chekhovskoi, G.I. Stavrovskii, A.B. Ivanov, High Temp. 9 (1971) 1090.
[12] O. Wilhelm, S.E. Pratsinis, D. Perednis, L.J. Gauckler, Thin Solid Films 479 (2005) 121.
[13] U.P. Muecke, N. Lüchinger, L. Schlagenhauf, L.J. Gauckler, submitted to Thin Solid Films (2006).
[14] S.A.A. Mansour, Thermochim. Acta 228 (1993) 173.
[15] N.A. Fuchs, The Mechanics of Aerosols, Pergamon Press, Oxford, 1964.
[16] J.R. Brock, J. Colloid Sci. 17 (1962) 768.
[17] R. Clift, J.R. Grace, M.E. Weber, Bubbles, Drops and Particles, Academic Press, New York, 1978.
[18] S. Nishio, M. Hirata, in: National Research Council of Canada (Ed.), International Heat Transfer Conference 6, Toronto, Canada, August 7–11, 1978, Hemisphere, Washington, 1978, p. 245.
[19] J.D. Bernardin, C.J. Stebbins, I. Mudawar, Int. J. Heat Mass Transfer 40 (1997) 247.
[20] J.D. Bernardin, C.J. Stebbins, I. Mudawar, Int. J. Heat Mass Transfer 40 (1996) 73.
[21] T.Y. Xiong, M.C. Yuen, Int. J. Heat Mass Transfer 34 (1991) 1881.
[22] N. Nagai, S. Nishio, Exp. Therm. Fluid Sci. 12 (1996) 373.
[23] J.D. Bernardin, I. Mudawar, C.B. Walsh, E.I. Franses, Int. J. Heat Mass Transfer 40 (1997) 1017.
[24] K.J. Baumeister, F.F. Simon, J. Heat Transf.-Trans. ASME 95 (1973) 166.
[25] Y. Ge, L.S. Fan, Phys. Fluids 17 (2005).
[26] G. Vazquez, E. Alvarez, J.M. Navaza, J. Chem. Eng. Data 40 (1995) 611.
[27] Knovel Critical Tables, Knovel, 2003.